

## The Latest Results from AMS on the International Space Station

---

**Samuel Ting**<sup>1</sup>

*Massachusetts Institute of Technology  
77 Massachusetts Avenue, Cambridge MA 02139, US  
E-mail: Samuel.Ting@cern.ch*

In four years on the International Space Station, the AMS experiment has collected more than 65 billion cosmic rays up to TeV energies. The latest results will be summarized.

*The 34th International Cosmic Ray Conference  
30 July- 6 August, 2015  
The Hague, The Netherlands*

---

<sup>1</sup>Speaker

### 1.Introduction

The Alpha Magnetic Spectrometer (AMS) was launched on NASA’s space shuttle Endeavour and installed on the International Space Station (ISS) on May 19, 2011 (see Figure 1). The experiment has dimensions of 5m x 4m x 3m and weighed 7.5 tons. The objectives of the experiment include the precision search for the origin of dark matter, antimatter, and cosmic rays as well as to explore the universe for new phenomena.

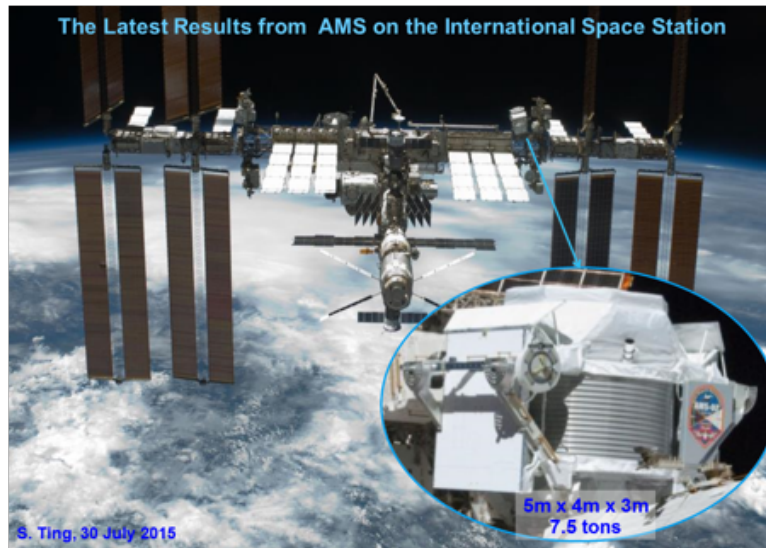


Figure 1: The Alpha Magnetic Spectrometer (AMS) on the International Space Station (ISS).

### 2.The Alpha Magnetic Spectrometer

As seen in Figure 2, the AMS detector consists of a permanent magnet surrounded by an array of particle detectors to measure the energy, momentum and charge of the passing particles and nuclei.

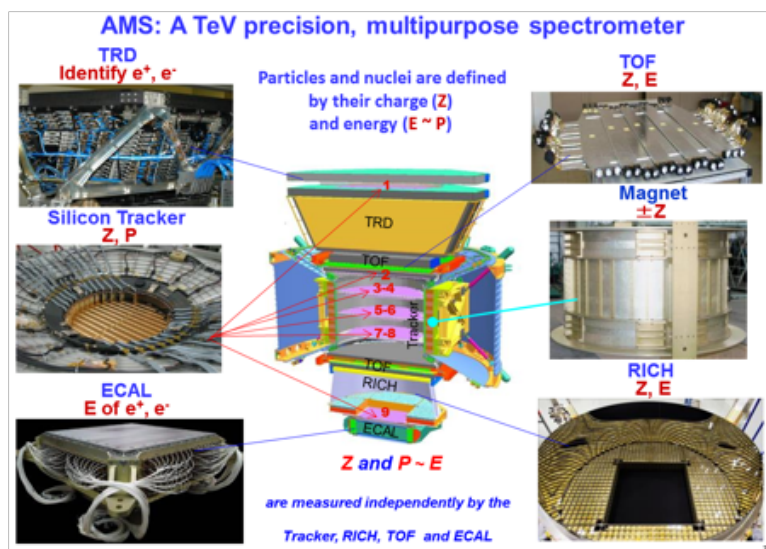


Figure 2: AMS is a TeV precision, multipurpose spectrometer.

POS (ICRC2015) 036

AMS involves an international collaboration of 16 nations sponsored by the U.S. Department of Energy (DOE), see Figure 3.

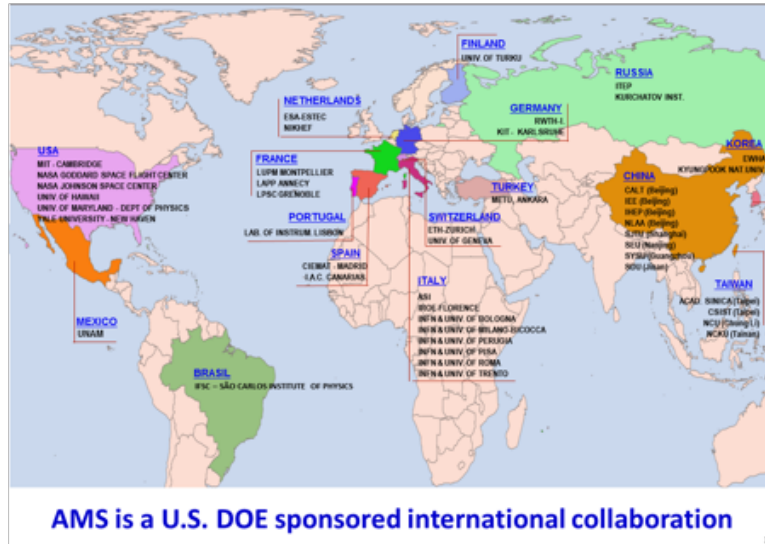


Figure 3: The AMS Collaboration. Institutes from Brazil and Turkey have recently joined.

The Transition Radiation Detector (TRD) is located at the top of the AMS detector (see Figure 4). Its purpose is to identify electrons and positrons by Transition Radiation while rejecting protons at a level of  $10^3$  and to distinguish nuclei by their  $dE/dx$ . Above and below the magnet bore are the Upper and Lower Time of Flight (TOF) counters. The purposes of this detector are to provide a trigger to AMS, to determine the direction and velocity of incoming particles and to measure their charge via  $dE/dx$  (see Figure 5). Within the magnet bore and above and below the magnet are a total of 9 precision silicon tracker planes, L1 to L9, with 200,000 channels aligned to 5 microns (see Figure 6). The purpose of the tracker, together with the magnet, is to measure the sign of the charge and momentum of the particles with unprecedented accuracy (a coordinate resolution of 10 microns). Anti-Coincidence Counters (ACC or Veto), with a measured efficiency of 0.99999, surround the tracker in the magnet bore. They reject cosmic rays entering AMS from the side. Below the Lower Time of Flight counters are the Ring Image Cherenkov counter (RICH) and Electromagnetic Calorimeter (ECAL). The RICH, with its 10,880 photo-sensors, measures the charge and velocity of passing particles (see Figure 7). Both are calculated from the geometrical shapes, circles or rings, generated by the Cherenkov effect. The RICH measures particle velocities with an accuracy of 0.1%. The ECAL is a 3-dimensional imaging instrument made of 1,200 lbs of lead sandwiched with 50,000 scintillating fibers, providing a measurement with  $17 X_0$  (see Figure 8). It measures the energy and direction of trillion electron volt (TeV) light rays and electrons with high precision (the energy resolution is  $\sim 2\%$ ), rejects protons at the level of  $10^4$  and measures the incident angle of energetic ( $>100$  GeV) electrons to  $0.5^\circ$ .

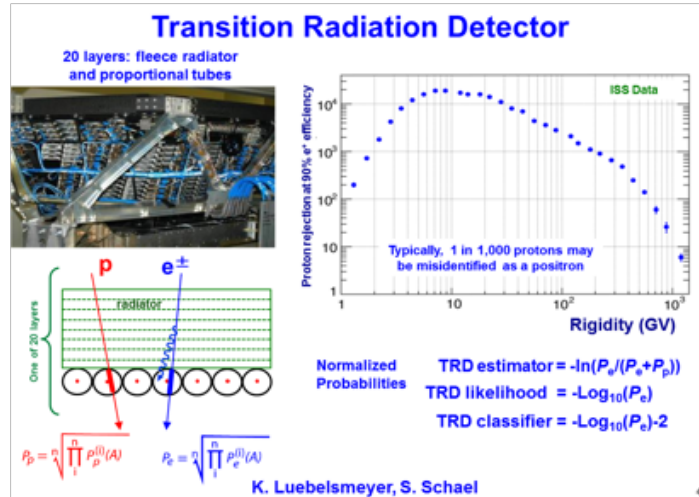


Figure 4: The AMS Transition Radiation Detector. The TRD estimator, likelihood and classifier are ways to distinguish electrons from protons. Prof. Luebelsmeyer and Schael are the leaders of this project.

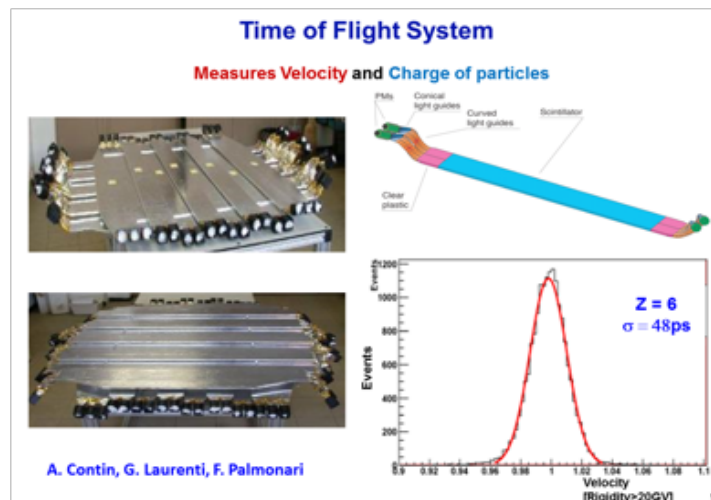


Figure 5: The AMS Time of Flight system. Shown are the construction principals, the final detector and the measured time resolution. Prof. Contini, Laurenti and Palmonari are the leaders of this project. A. Kounine made major contributions to the electronics.

POS (ICRC2015) 036

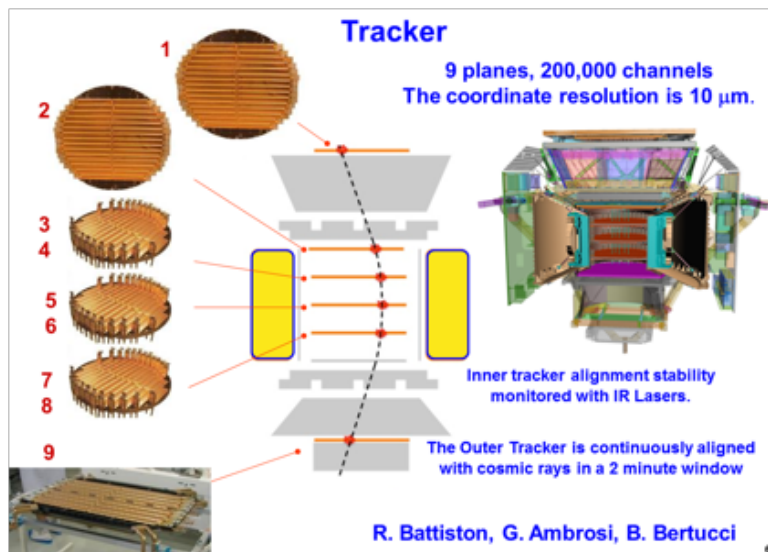


Figure 6: The AMS silicon microstrip tracker. Prof. Battiston, Ambrosi and Bertucci are the leaders of this project.

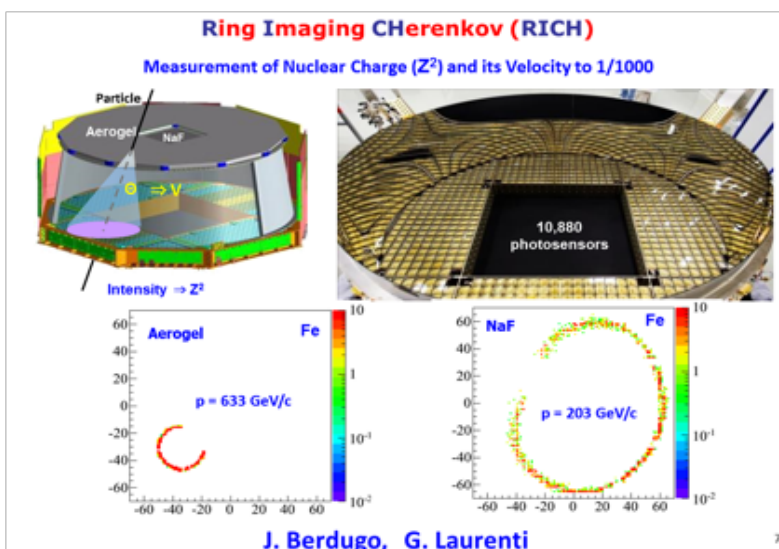


Figure 7: The AMS Ring Imaging Cherenkov Counter (RICH). Prof. Berdugo and Laurenti are the leaders of this project.

POS (ICRC2015) 036

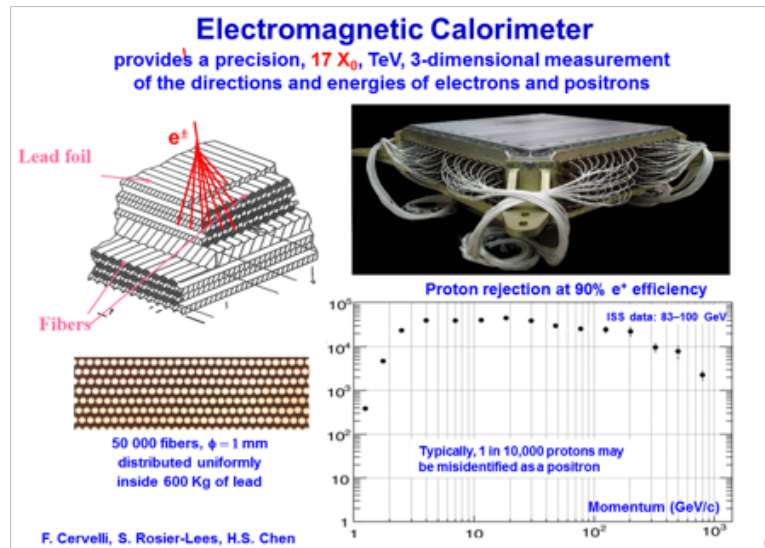


Figure 8: The AMS Electromagnetic Calorimeter (ECAL). Prof. Cervelli, Rosier-Lees, J. P. Vialle and Chen are the leaders of this project.

The AMS electronics system consists of 300,000 readout channels and 650 microprocessors. It was designed under the leadership of Dr. M. Capell of MIT, including V. Koutsenko, A. Kounine, A. Lebedev, X. Cai, and built in Taiwan with the support of Prof. S.C. Lee of Academia Sinica and CSIST. It reads out and controls the entire detector. Extensive testing of all the electronics components and boards was carried out before construction to ensure the electronics will withstand the stresses of launch (static and vibration loads), rapid depressurization without outgassing under vacuum, radiation exposure to about a Krad/year and remain electromagnetically compatible with the ISS and the sensitive detectors of AMS itself. In particular, components that met the performance and thermal requirements were subjected to heavy ion beam tests to probe for single event effects (bit flips or latch ups) and selected accordingly. Overall, after four years of operation, the electronics system has performed exceedingly well.

Before launch to the ISS, AMS was tested extensively at the CERN test beam (see Figure 9) with electrons, positrons, protons, and pions (to simulate high energy protons). In total, more than 2000 combinations of incident angle and location were tested. The measured proton rejection at 400 GeV was larger than  $10^6$ . The test beam results are used with AMS in space to monitor the detector performance and also in the data analysis to verify the quality of the data from space.

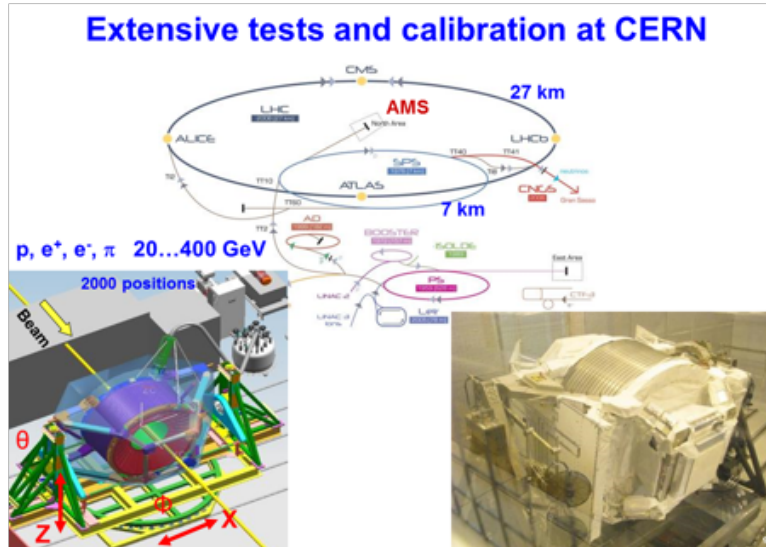


Figure 9: AMS in the test beam at CERN (2010).

To maintain the detector resolution and to mitigate the hostile thermal environment on the ISS, a Thermal Control System with 1,118 temperature sensors and 298 heaters keeps the detector safely within its operational range. Prof. Cheng Lin of Shandong University made a major contribution to this project. The Tracker has its own Thermal Control System (TTCS) that keeps the Tracker temperature stable at  $10 \pm 3^\circ\text{C}$  and is described in a separate section.

The successful operation of AMS depends on the proper monitoring and control of the thermal system and electronics system. This is performed from the AMS Payload Operations and Control Center (POCC) at CERN on a 24/7/365 basis. As indicated in Figure 10, to date more than 68 billion cosmic rays have been collected with AMS on the ISS.



Figure 10: AMS on ISS, seen from above.

### 3. Analysis and Results

As mentioned, after over 4 years onboard the International Space Station, AMS has recorded over 68 billion charged cosmic ray events; far more than in the entire history of cosmic ray physics. These events are being analyzed at the AMS Science Operations Center located at CERN and at AMS universities around the world (see Figure 2). At least two independent groups are organized within the AMS Collaboration to analyze the data for each physics topic. Some of the leaders of the analysis effort are shown in Figure 11.

Recent results from AMS provide a deeper understanding of the nature of high-energy cosmic rays and shed more light on the existence and nature of dark matter. As indicated in Figure 12, dark matter collisions will produce an excess of antimatter particles (positrons, antiprotons, etc.) and this excess can be most easily studied by measuring the positron fraction. Ordinary cosmic ray collisions result in the positron fraction (flux of positrons divided by the flux of electrons and positrons) decreasing steadily with energy and the antiproton/proton ratio tapering off. Different models on the nature of dark matter predict different behavior of the positron fraction excess above the positron fraction expected from ordinary cosmic ray collisions. Depending on the nature of dark matter, the excess of the positron fraction has a unique signature.

As shown in Figure 13, three AMS detectors play a key role in the measurements of positrons and electrons. The TRD identifies electrons and positrons from the background of protons. The tracker measures the momentum of the charged cosmic ray and the charge sign, separating electrons from positrons. The shower shape in the ECAL also distinguishes electromagnetic electrons and positrons from the background of hadronic protons and this is enhanced by matching the momentum measured with the magnet and tracker with the energy measured in the ECAL. The separation of the TRD and the ECAL by the magnetic field ensures that the rejection power of the two detectors are independent.

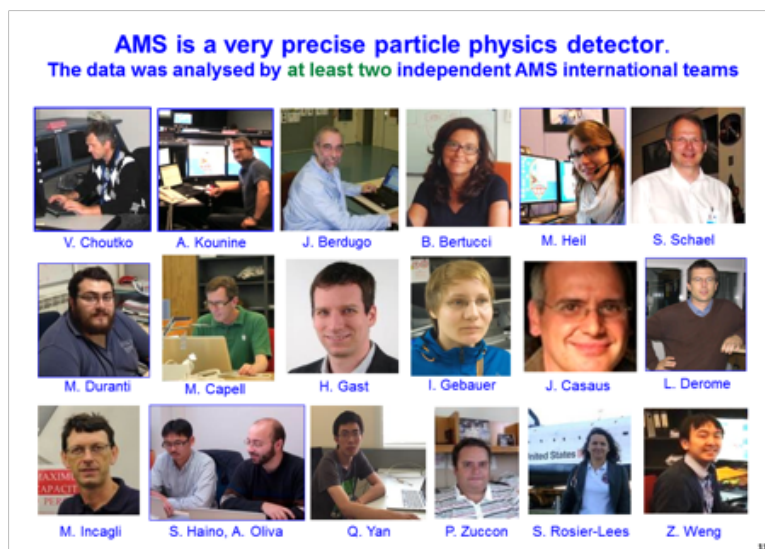


Figure 11: Some of the leaders of the AMS analysis efforts.



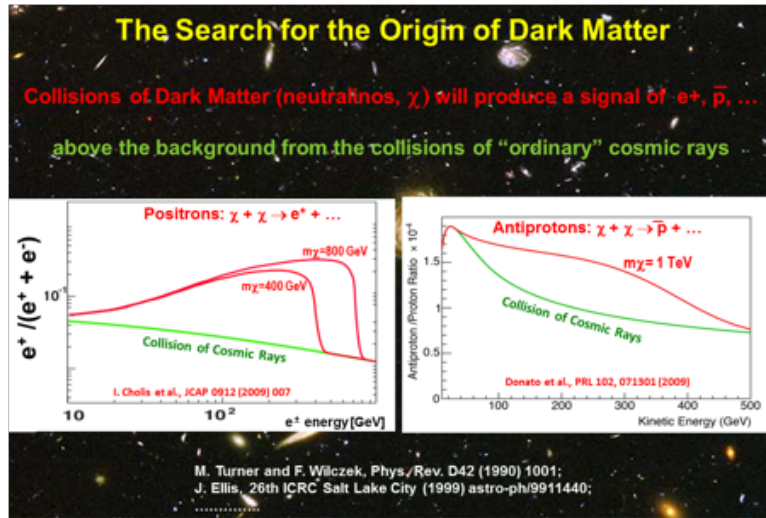


Figure 12: The Search for the Origin of Dark Matter with charged cosmic rays. Also mentioned are the original papers on this subject.

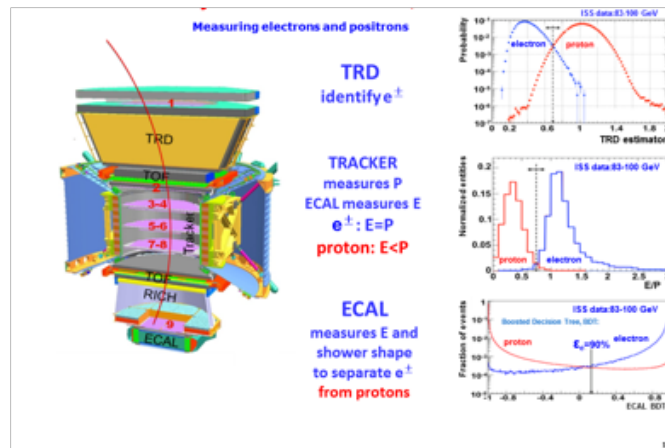


Figure 13: The principals separating electrons and positrons from hadrons, independently by TRD, by tracker and by ECAL. The individual rejection power of each is shown on the right.

In addition to using the techniques mentioned above, the rejection power of the TRD alone is sufficient to measure the positron fraction. As shown in Figure 14, this allows the verification of the positron fraction reported by AMS using an independent sample of events, namely those outside the ECAL acceptance. This result is in excellent agreement with the results reported below.

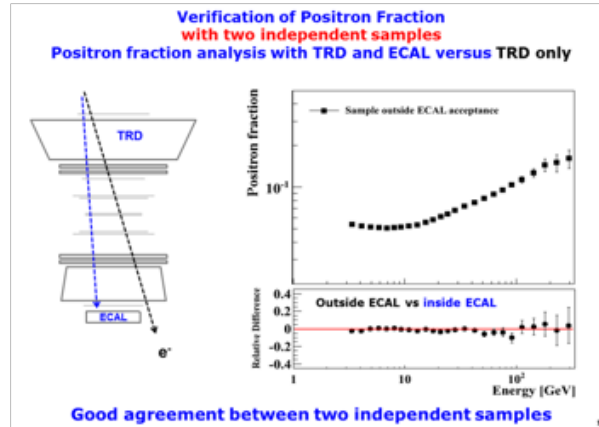


Figure 14: Verification of the published AMS positron fraction with an independent event sample outside of the ECAL acceptance.

The first AMS publication on the positron fraction was based on 6.8 million positron and electron events. As shown in Figure 15, it was selected by the American Physical Society as an Annual Highlights in Physics.



Figure 15: The first AMS publication which was on the positron fraction.

Our second publication was based on the increased statistics of 10.9 million positron and electron events and extended the energy range of the positron fraction measurement to 500 GeV as shown in Figure 16 [1]. This allowed the methodical examination of the six characteristics of the positron fraction indicated in Figure 17. Figures 18, 19, 20, 21, and 22 show the results of these examinations of this previously unobserved behavior. Figure 18 shows that at low energies our measured positron fraction is very similar to expectations from ordinary cosmic rays. As seen in Figure 18, above 7.8 GeV, the measured positron fraction increases quickly

whereas the model predicts a slow decrease. Figure 19 shows our measured positron fraction, its rate of increase with energy and that there are no sharp peaks in the spectrum.

To examine the energy dependence of the positron fraction quantitatively in a model independent way, straight line fits were performed over the entire energy range with a sliding energy window, where the width of the window varies with energy to have sufficient sensitivity to the slope. Each window covers about eight bins, at energies above 200 GeV it covers three bins. The variation of the slope of the positron fraction from 4 GeV upwards is shown in the upper half of Figure 20. As seen in the figure, above 30 GeV the slope decreases logarithmically with energy. Fitting the change of the slope as a function of energy above 30 GeV with a two parameter fit [slope =  $c \log (E/E_0)$  where  $c$  is the normalization and  $E_0$  is the energy at which the slope crosses zero, that is, the energy at which the positron fraction reaches its maximum] results in a determination of  $E_0 = 275 \pm 32$  GeV with a  $\chi^2/\text{d.f.} = 3.9/12$  taking correlations into account. The result of the fit is shown as a solid blue line in Figure 20. This confirms our observation from Figure 19 that above  $> 200$  GeV the positron fraction is no longer increasing with energy.

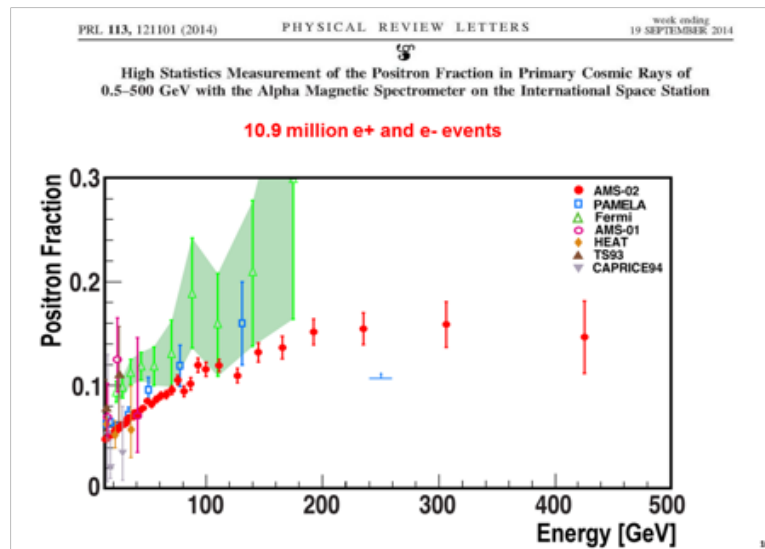


Figure 16: The positron fraction measured with increased statistics and to higher energy.

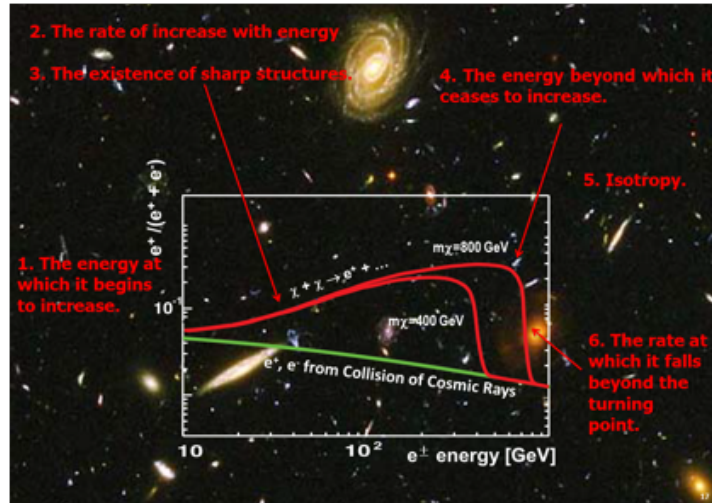


Figure 17: Six characteristics of the behavior of the positron fraction from different models versus energy.

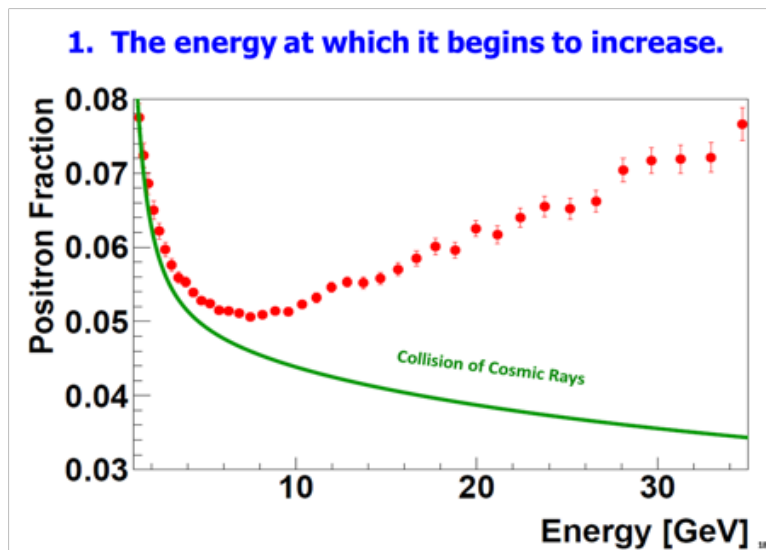


Figure 18: The first characteristic.

POS (ICRC2015) 036

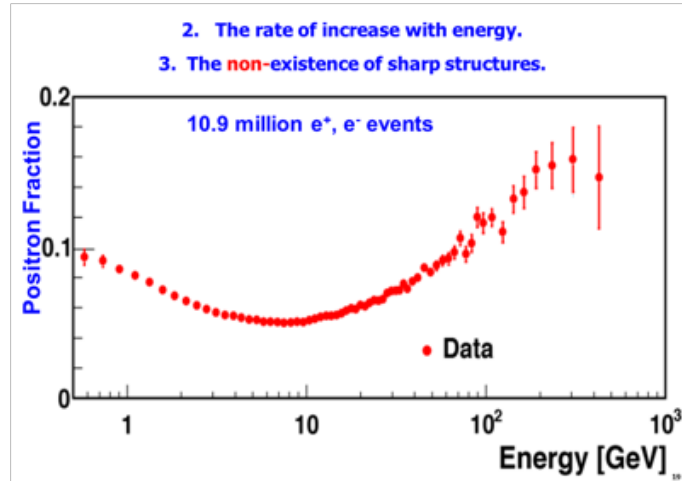


Figure 19: The second and third characteristics.

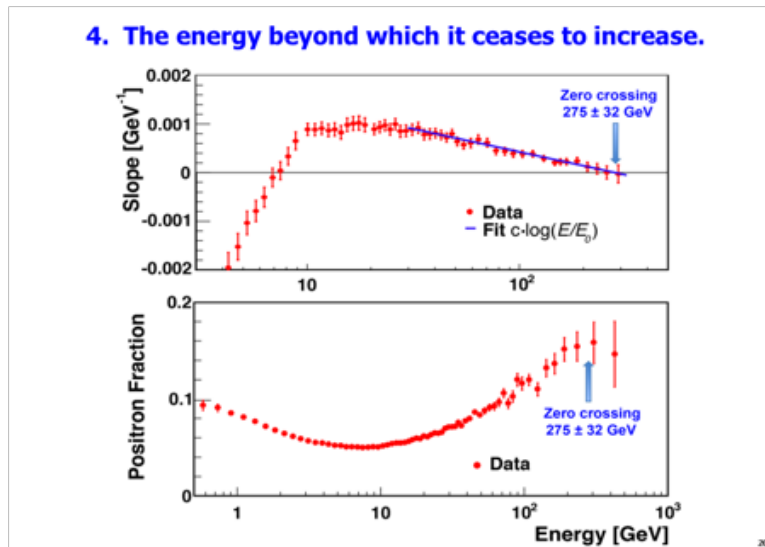


Figure 20: The fourth characteristic. (upper) The slope of the positron fraction vs energy over the entire energy range (the values of the slope below 4 GeV are off scale). The line is a logarithmic fit to the data above 30 GeV. (lower) The positron fraction measured by AMS. The error bars are the quadratic sum of the statistical and systematic uncertainties.

The anisotropy is calculated from the arrival directions of electrons and positrons which are used to build up a sky map in galactic coordinates shown on the left of Figure 21. The fluctuations of the observed positron to electron ratio are described using a spherical harmonic expansion. From the coefficients of the first moment of the expansion an upper limit on the amplitude of the dipole moment is found to be  $\delta < 0.030$  at the 95% C.L.

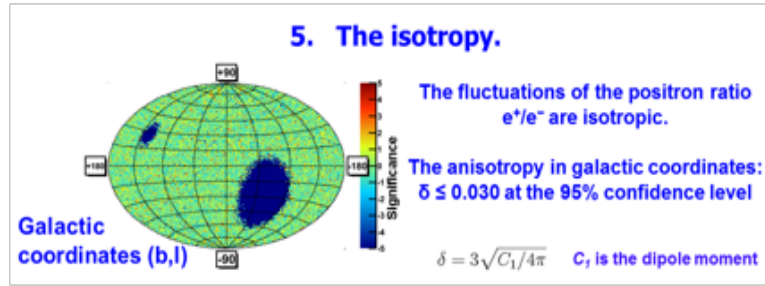


Figure 21: An upper limit on the fifth characteristic.

To ascertain the origin of the positron fraction behavior, measurements are continuing with AMS. Figure 22 shows the expectation for 10 more years of measurements which should help us to determine if the positron fraction falls off rapidly as predicted by models of Dark Matter collisions or falls off slowly, as expected from pulsars or other astrophysical sources. The precision measurements of the positron and electron anisotropies (characteristic 5 of Figure 17, see also Figure 21) will also help to distinguish the different possible sources.

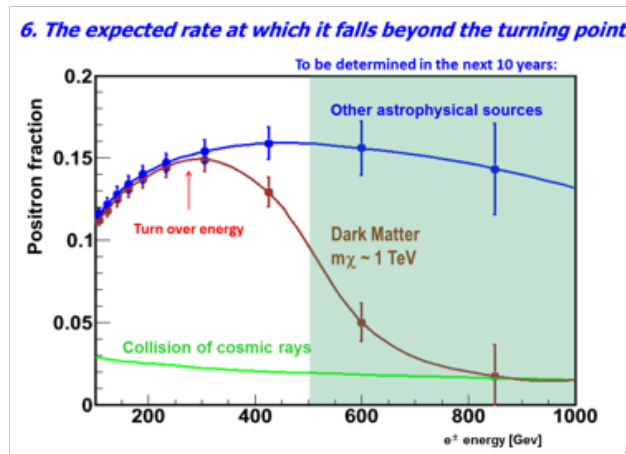


Figure 22: Towards an answer to the sixth characteristic, projected AMS measurement of the behavior of the positron fraction in ten years.

The origin of these phenomena can only be definitively determined by continuing to collect data up to the TeV region. In addition to producing an excess of positrons, it is expected for many types of dark matter that they would also produce an excess of antiprotons (see Figure 12, right). AMS has measured the antiproton/proton ratio as shown in Figure 23 together with recent measurements [1]. AMS has extend the energy range and increased the precision. As shown in Figure 24, the ratio by AMS is larger than that expected from theoretical models based on data collected before the AMS measurements.

The origin of these phenomena can only be definitively determined by continuing to collect data up to the TeV region.

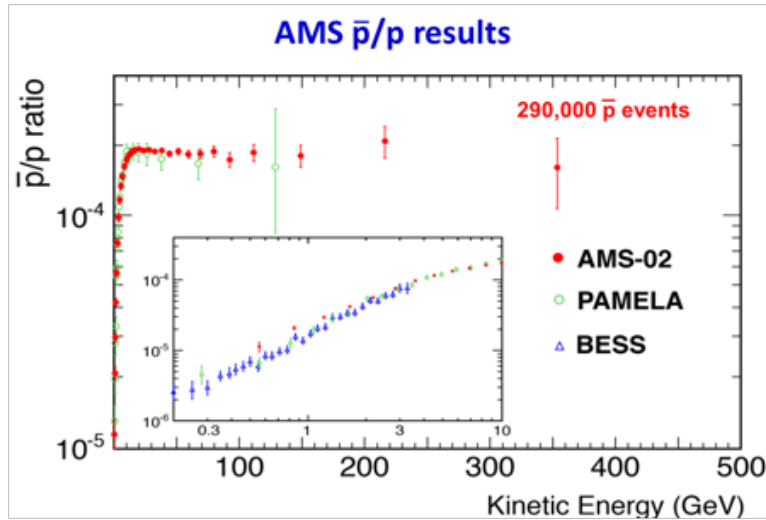


Figure 23: The antiproton/proton ratio measured by AMS based on 290,000 antiproton events. The insert shows, for comparison, our measurements and other measurements at lower energies (<10 GeV).

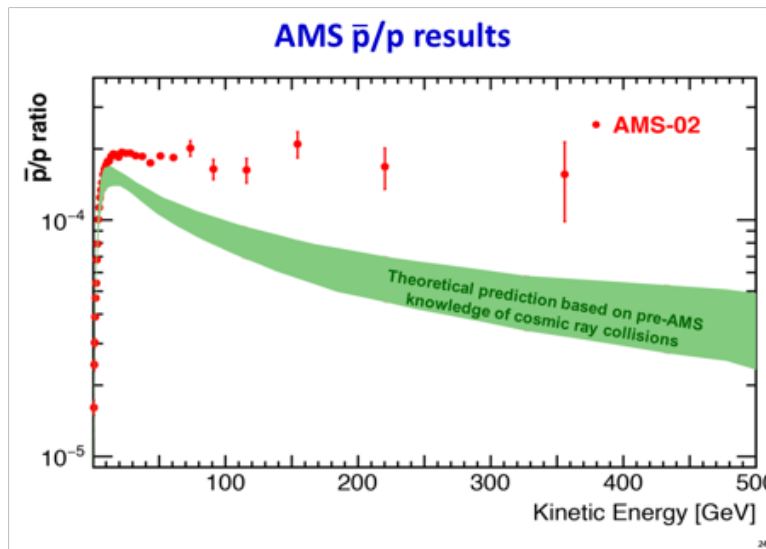


Figure 24: The antiproton/proton ratio on a linear energy scale.

In *Electron and Positron Fluxes in Primary Cosmic Rays Measured with the Alpha Magnetic Spectrometer on the International Space Station*, M. Aguilar, et al., Phys. Rev. Lett 113, 121102 (2014) precision measurements by AMS of the primary cosmic ray electron flux in the energy range 0.5 to 700 GeV and the positron flux in the range 0.5 to 500 GeV are presented. Figure 25 shows the measurements previously reported and Figure 26 show the AMS measurements [2]. The AMS measurements, based on 9.2 million electron and 0.6 million positron events, show that the electron flux and the positron flux each require a description beyond a single

power law spectrum,  $\Phi=C \cdot E^\gamma$ , where  $\gamma$  is the spectral index and  $C$  is a normalization constant. Both the electron flux and the positron flux change their behavior at  $\sim 30$  GeV, but the fluxes are significantly different in their magnitude and energy dependence. As shown in Figure 27, between 20 and 200 GeV the positron spectral index is significantly harder than the electron spectral index. These precise measurements show that the rise in the positron fraction above 10 GeV is due to the hardening of the positron spectrum and not to the softening of the electron spectrum. The determination of the differing behavior of the spectral indices versus energy is a new observation and provides important information on the origins of cosmic ray electrons and positrons.

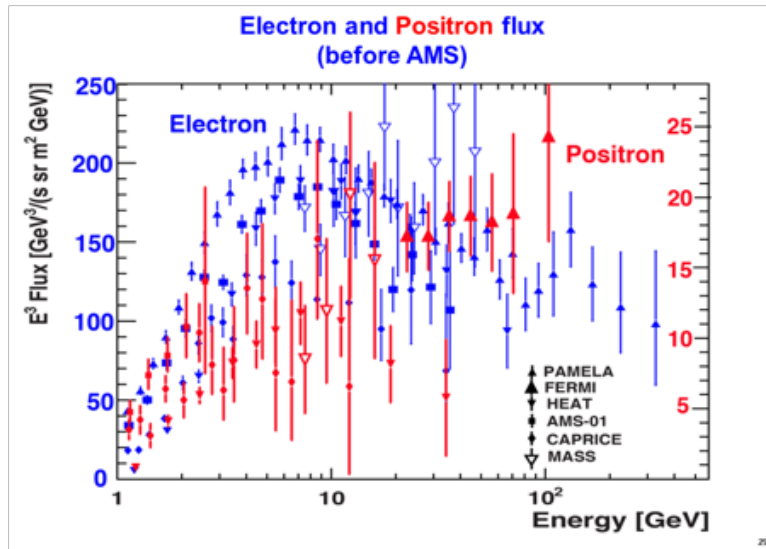


Figure 25: Measurements of the electron and positron fluxes multiplied by  $E^3$  before AMS.

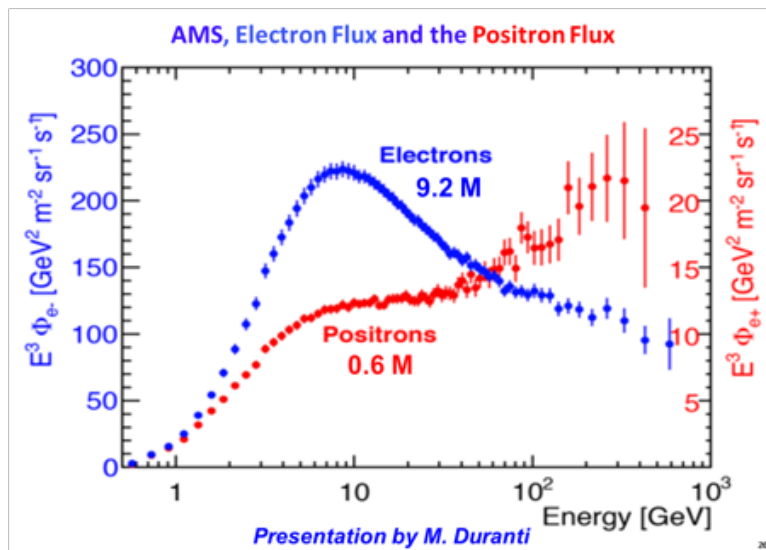


Figure 26: The AMS measurements of the electron and positron fluxes multiplied by  $E^3$ .



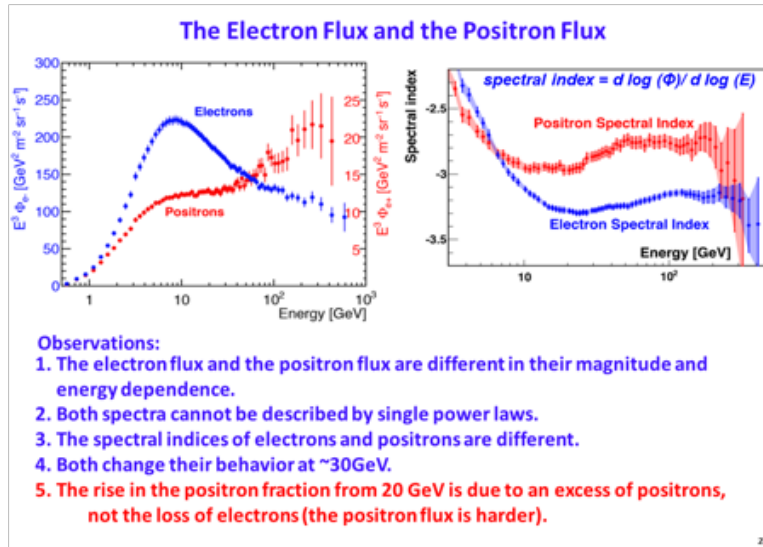


Figure 27: Observations from the AMS measurements of (left) the electron and positron fluxes multiplied by  $E^3$  and (right) their spectral indices as a function of  $E$ .

*Precision Measurement of the ( $e^+ + e^-$ ) Flux in Primary Cosmic Rays from 0.5 GeV to 1 TeV with the Alpha Magnetic Spectrometer on the International Space Station*, M. Aguilar et al., Phys. Rev. Lett 113, 221102 (2014) was also recently published by AMS. The measured flux of electrons plus positrons is shown in Figure 28 [2]. Compared to all the previous publications of this spectrum, this paper greatly improved the precision by reducing the statistical and systematic errors. Our measurement indicates that the flux is smooth, i.e., no structures were observed, in contrast to previous publications.

This measurement reveals new and distinct information. As seen in Figure 29, from 30.2 GeV to 1 TeV, the flux can be described by a single power law with  $g = -3.170 \pm 0.008$  (stat+sys)  $\pm 0.008$  (energy scale) and this is different from the behavior of the individual electron and positron fluxes and spectral indices shown in Figure 27.

Together with our publications on  $e^+$  and  $e^-$  fluxes and the positron fraction it is now possible to conduct accurate comparisons with various particle physics and astrophysics models including the minimal model.

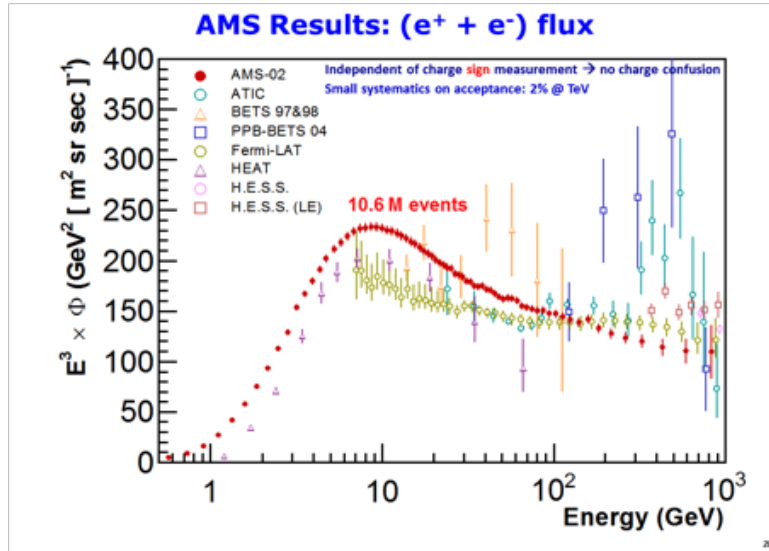


Figure 28: The AMS measurement of the (electron + positron) flux based on 10.6 million events together with recent measurements.

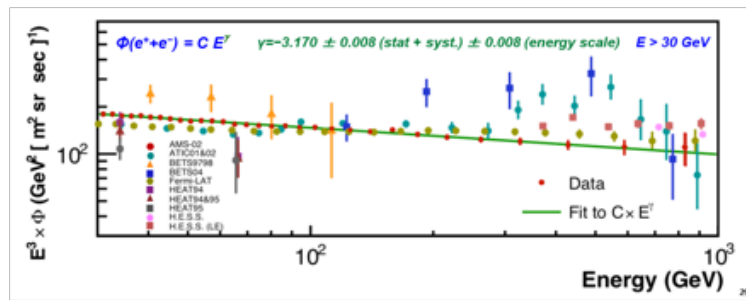


Figure 29: The AMS measurement of the (electron + positron) flux together with recent measurements multiplied by  $E^3$ .

As presented in Figure 30, to fully understand the behavior of the positrons, electrons, the positron fraction, and the antiproton/proton ratio, it is necessary to have an accurate understanding of the behavior of all cosmic rays including protons, helium, lithium, etc. In addition, the study of these different nuclei may reveal interesting features in themselves. As shown in Figure 31, AMS, which makes multiple independent determinations of the nuclear charge magnitude, is starting to report these measurements.

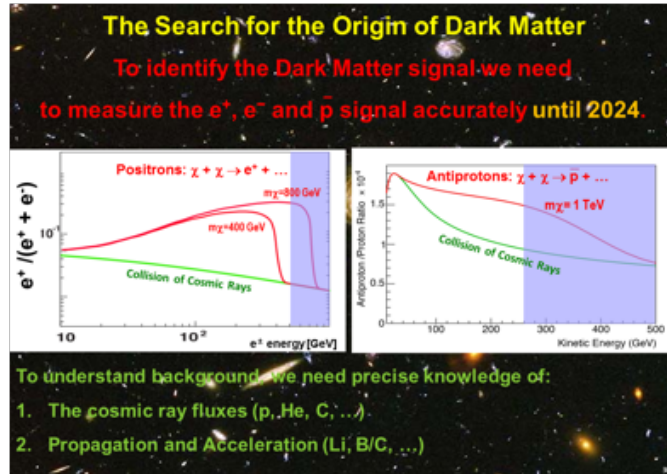


Figure 30: The underpinnings of the Search for Dark Matter with charged cosmic rays.

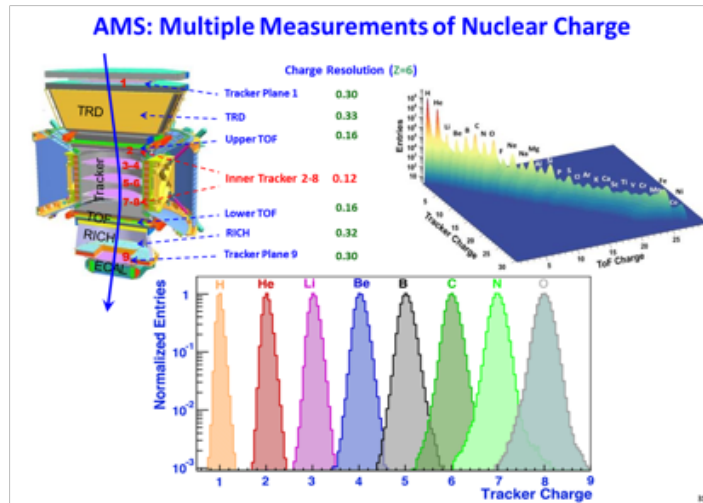


Figure 31: AMS provides multiple measurements of the nuclear charge. The charge resolution for Z=6, carbon, of the seven different measurements are listed. Also shown are the measurement of the periodic table from the correlation of two of these measurements and the normalized charge resolution for light nuclei by the tracker alone. As seen, the charge overlap is minimal.

As shown in Figure 32, we reported a precise measurement of the proton flux in primary cosmic rays with rigidity (momentum/charge) from 1 GV to 1.8 TV based on 300 million events [3]. Knowledge of the rigidity dependence of the proton flux is important in understanding the origin, acceleration and propagation of cosmic rays. This publication presented for the first time the detailed variation with rigidity of the flux spectral index. The spectral index shows that the proton flux deviates from a single power law and progressively hardens at high rigidities.

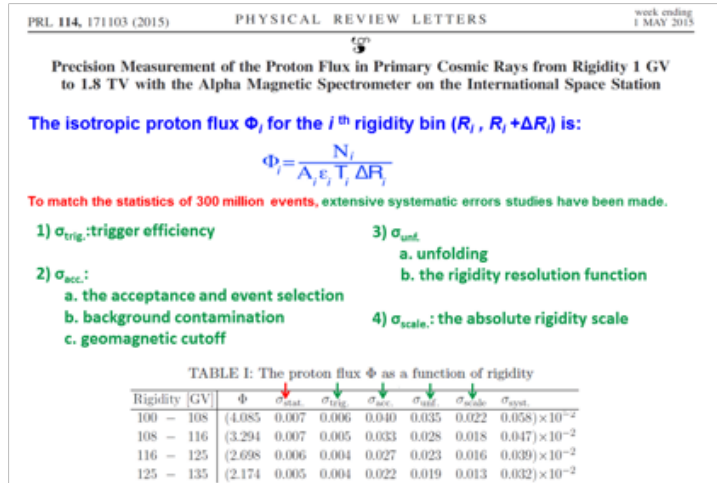


Figure 32: Measuring the proton flux with AMS. Shown in this figure are the extensive studies of systematic errors from trigger efficiency, from the acceptance, from unfolding and from the rigidity scale.

Figure 33 shows the result of our measurement based on 300 million events. It shows that the behavior of the proton spectrum cannot be explained by a single power law. As seen for the first time, this change of behavior occurs smoothly at  $R \sim 300$  GV.

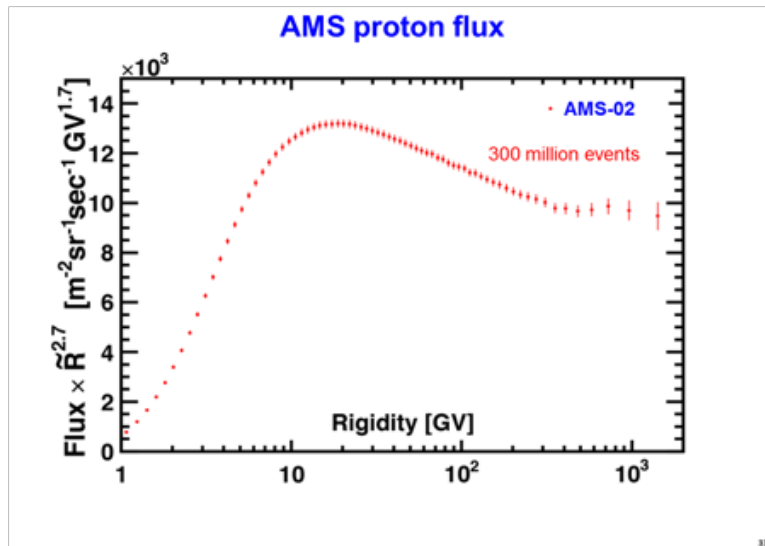


Figure 33: The proton flux measured with AMS multiplied by  $R^{2.7}$ .

Figure 34 provides an analytical study of the dependence of the proton spectrum on rigidity. Figure 34 shows that the spectrum fits well with a double power law function  $\Phi=C \cdot (R/45\text{GV})^\gamma \cdot (1+(R/R_0)^{\Delta\gamma/s})^s$ . It also shows a significant deviation from a single power law ( $\Delta g = 0$ ) prediction.

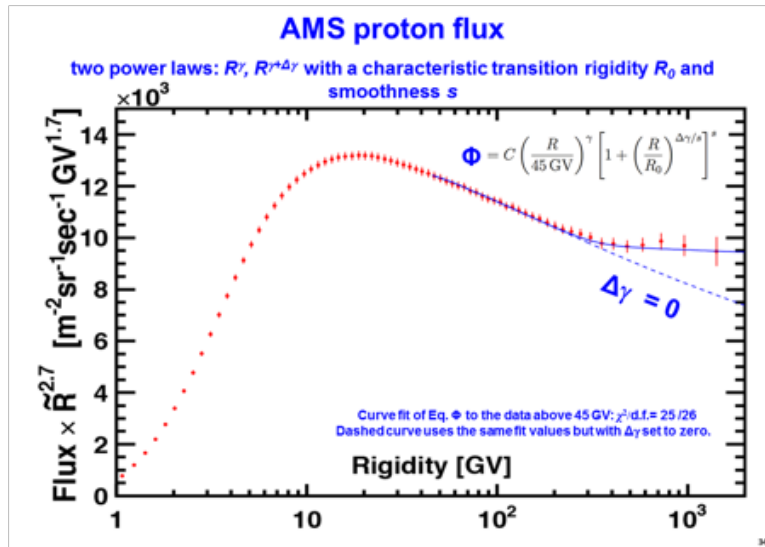


Figure 34: The AMS proton flux multiplied by  $R^{2.7}$  and fit with a double power law.

Figure 35 provides a model independent and accurate measurement of the spectral index  $g$  of the proton flux  $\Phi=C \cdot R^\gamma$ . As seen, the spectral index is neither a constant nor changes abruptly, as was previously reported, but varies smoothly as a function of rigidity. This is an important observation reported for the first time.

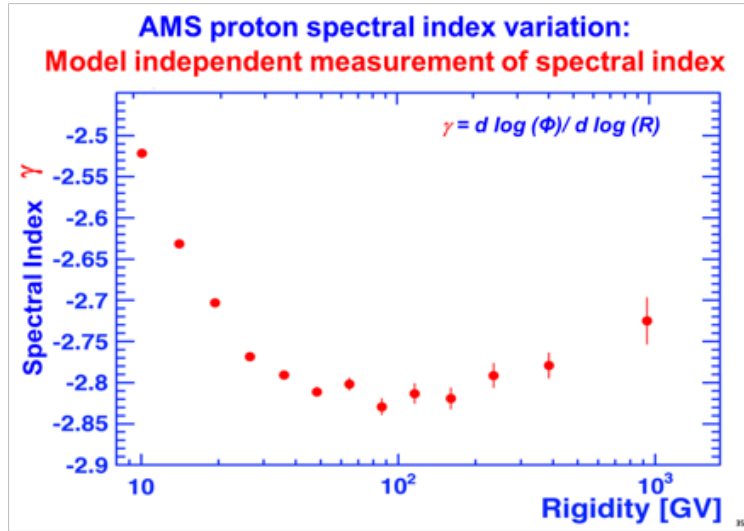


Figure 35: The variation of the proton spectral index measured by AMS.

Figure 36 shows the comparison of our data with previous published results in terms of kinetic energy. As seen, our result updates previous measurements in a significant way both in accuracy and rigidity dependence.

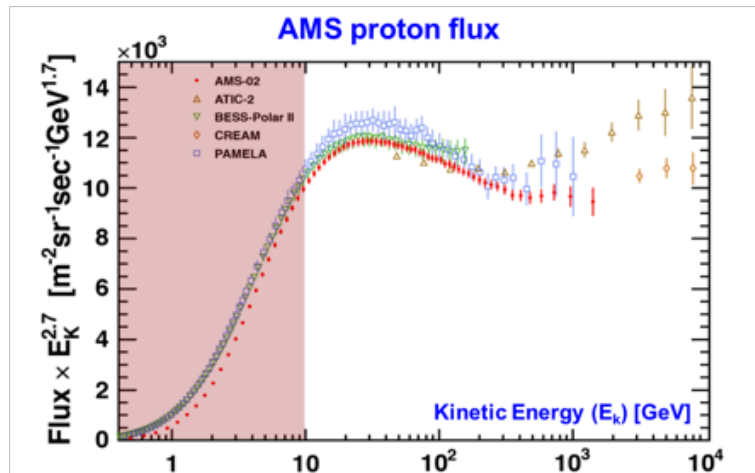


Figure 36: The AMS proton flux together with recent measurements multiplied by  $E^{2.7}$ .

Our next publication will be *Precision Measurement of the Helium Flux in Primary Cosmic Rays from Rigidities of 1.9 GV to 3 TV with the Alpha Magnetic Spectrometer on the International Space Station* (ed: M. Aguilar et al., Phys. Rev. Lett. 115, 211101 (2015)).

Helium nuclei in cosmic rays are believed to be mainly produced by Galactic sources such as supernova remnants. Precise knowledge of the helium spectrum in the GV-TV rigidity region provides important information on the origin, acceleration, and subsequent propagation processes of cosmic rays in the Galaxy. This paper reports results from a precise measurement of the helium flux in primary cosmic rays with rigidity from 1.9 GV to 3 TV based on 50 million events. This paper used the first 2.5 years of data taking. To obtain the best resolution at the highest energies, only events which passed through all 9 tracker layers were selected. The detailed variation with rigidity of the helium flux spectral index is presented for the first time. The spectral index progressively hardens at high rigidities. The magnitude of the helium spectral index is different from that of the proton spectral index, but the rigidity dependence of the fluxes is similar for helium and protons. Using our measurement of the proton flux with the same dataset, the paper also reports the characteristics of the ratio of the proton flux to the helium flux. Remarkably, the spectral index of the proton to helium flux ratio increases with rigidity up to 45 GV and then becomes constant; the flux ratio above 45 GV is well described by a single power law.

With 50 million helium events, the study of systematic errors becomes important. Much of the systematic error study is similar to that performed for the proton flux. Of particular importance in the case of helium, is the study of the acceptance.

To accurately determine the effect on the acceptance of helium interactions in the detector, we have developed a method to determine the magnitude and rigidity dependence of the survival probability of helium when traversing the detector materials, see Figure 37. We used a sample of cosmic rays collected with AMS horizontal, that is, when the ISS was oriented such that AMS was pointing within  $90^\circ \pm 10^\circ$  of the local zenith, a total of  $1.4 \times 10^5$  s, see Figure 38. As shown in Figure 39, particles which passed through the inner tracker layers from L8 to L2 were identified as helium,  $Z = 2$ , with the  $dE/dx$  measurements in those seven layers. We then measured the survival probability for these events traversing the materials from L2 to L1 (the upper TOF and TRD) by comparing the charge distributions between L2 and L1. Likewise, the survival probability from L8 to L9 was measured with AMS horizontal and this measurement agrees with the measurement made with data collected when AMS was in the nominal orientation. This also verifies the accuracy of the measurement of the survival probability between L2 and L1. Figure 40 shows the resulting estimation of the (helium on carbon) cross section compared to accelerator measurements.

To measure the flux of nuclei (He, Li, Be, B, C, O, ...) accurately, we need to know the interaction cross section of these nuclei with the materials in AMS.

Unfortunately, the interactions of nuclei with the materials in AMS could not be measured on the ground. This limits the accuracy to which we could measure the fluxes.

On ISS we have now a method to measure these interactions in space accurately.

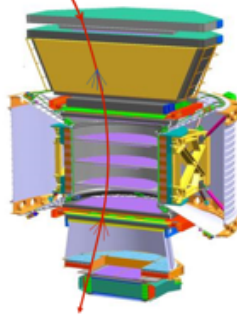


Figure 37: To match with the high statistics, we need to measure the interactions of nuclei.

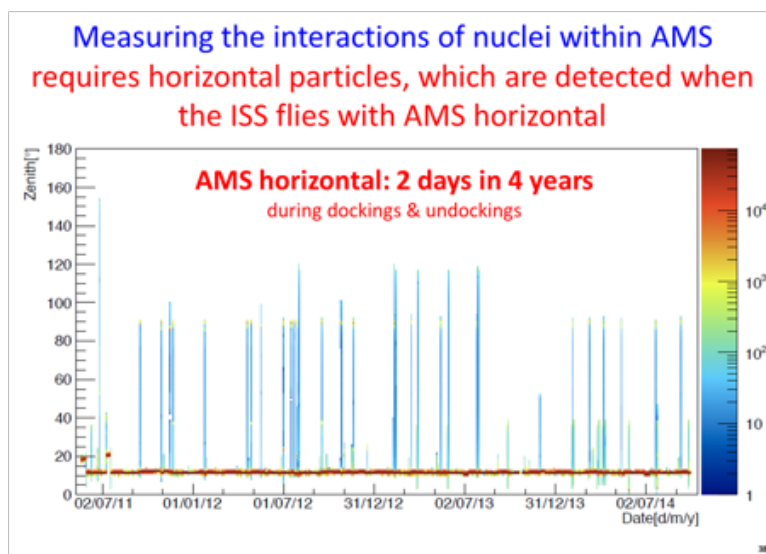
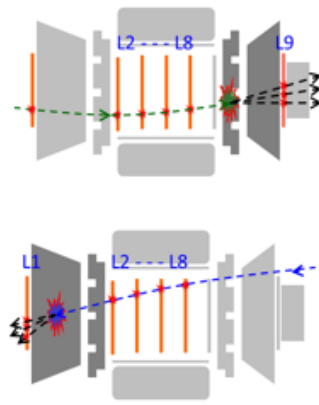


Figure 38: The zenith angle of AMS vs time.

Measuring the interactions of nuclei within AMS when AMS is flying horizontal



First, we use the seven inner tracker layers, L2-L8, to define beams of nuclei: He, Li, Be, B, ...

Second, we use left-to-right particles to measure the nuclear interactions in the lower part of the detector.

Third, we use right-to-left particles to measure the nuclear interactions in the upper part of detector.

Figure 39: Measuring the interactions of nuclei within AMS when it is horizontal.



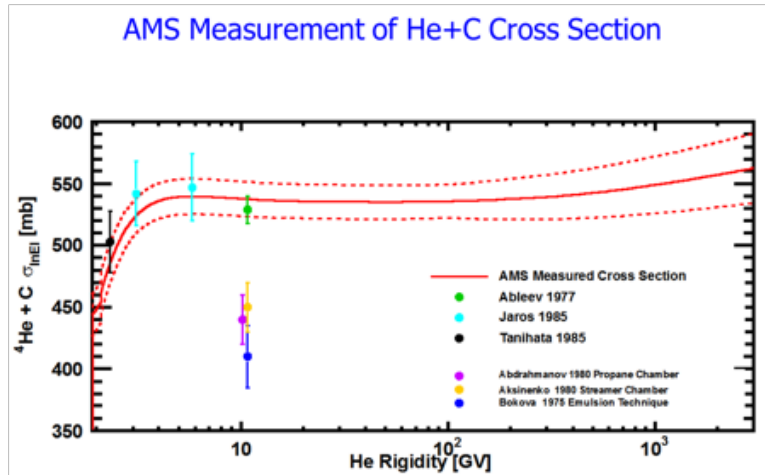


Figure 40: AMS measurement of the (He+C) cross section compared with accelerator measurements. The solid curve is the AMS result and the dashed lines represent the measurement errors.

Figure 41 shows the result of our measurement based on 50 million events [4]. It shows that the behavior of the helium spectrum cannot be explained by a single power law. Similarly to the proton flux, it shows for the first time that the change of behavior occurs smoothly at  $R \sim 300$  GV.

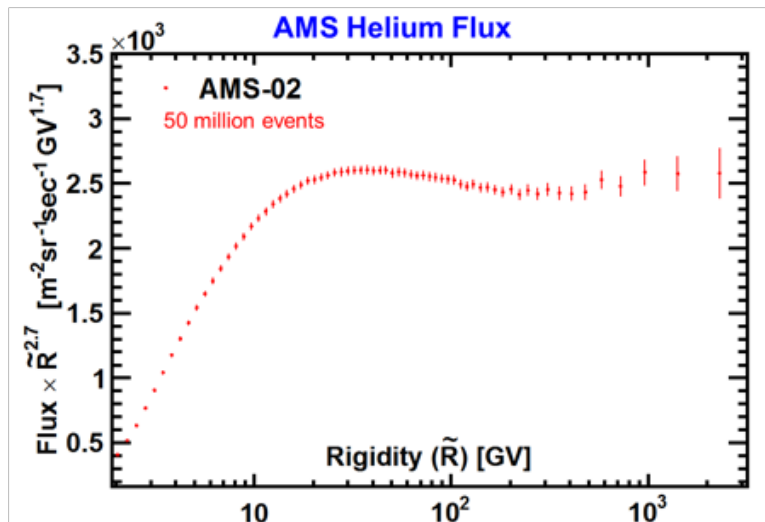


Figure 41: The helium flux measured with AMS multiplied by  $R^{2.7}$ .

Figure 42 provides an analytical study of the dependence of the helium spectrum on rigidity. It shows that the spectrum fits well with a double power law function  $\Phi=C\cdot(R/45\text{GV})^\gamma\cdot(1+(R/R_0)^{\Delta\gamma/s})^s$ . It also shows a significant deviation from a single power law ( $\Delta g = 0$  or  $R_0 \rightarrow \infty$ ) prediction

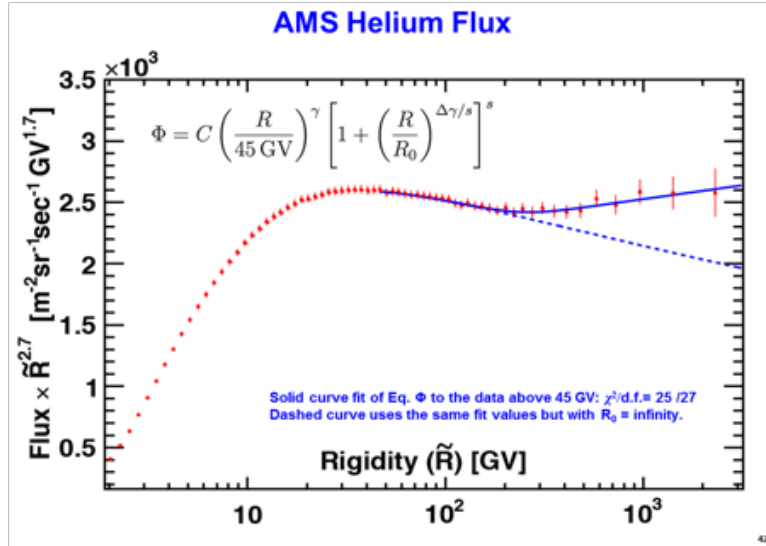


Figure 42: The AMS helium flux multiplied by  $R^{2.7}$  and fit with a double power law.

Figure 43 shows the comparison of our data with previous published results in terms of kinetic energy. Again, our result updates previous measurements significantly both in accuracy and rigidity dependence.

POS (ICRC2015) 036

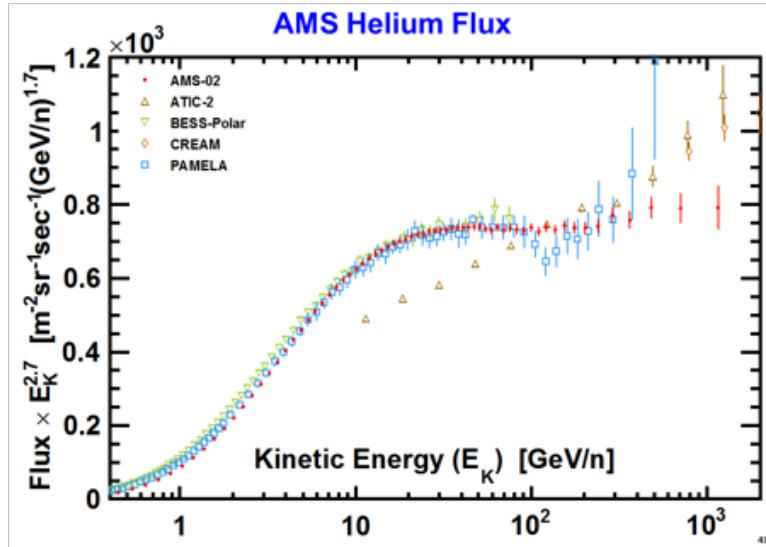


Figure 43: The AMS helium flux together with recent measurements multiplied by  $E^{2.7}$ .

Figure 44 provides a model independent and accurate measurement of the spectral index  $\gamma$  of the helium flux  $\Phi=C \cdot R^\gamma$  along with our measurement of the proton spectral index from Figure 35. As seen, the spectral indices are different in magnitude but exhibit similar functional behavior.

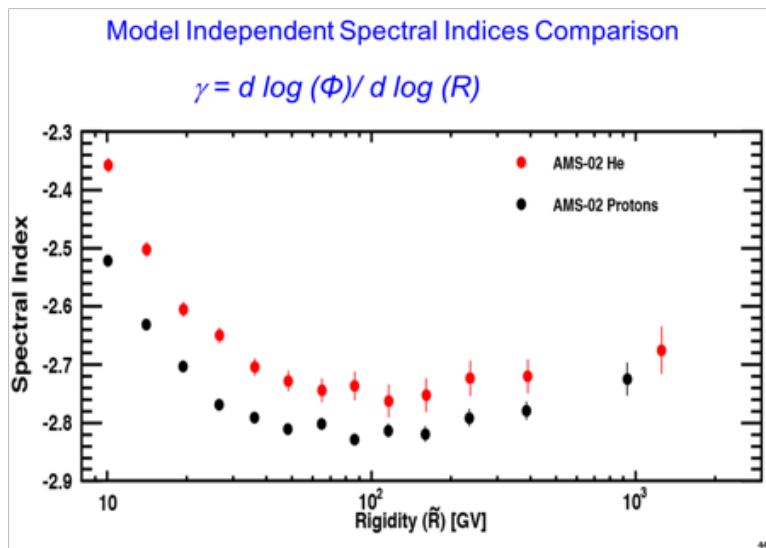


Figure 44: The AMS measurements of the proton and helium spectral indices.

Figure 45 shows the ratio of the proton flux to the helium flux from AMS compared with an important recent model prediction. The solid blue curve indicates a fit to the AMS data with a single power law,  $\Phi=C \cdot R^\gamma$ . As seen, above 45 GV the ratio is well described by a single power law.

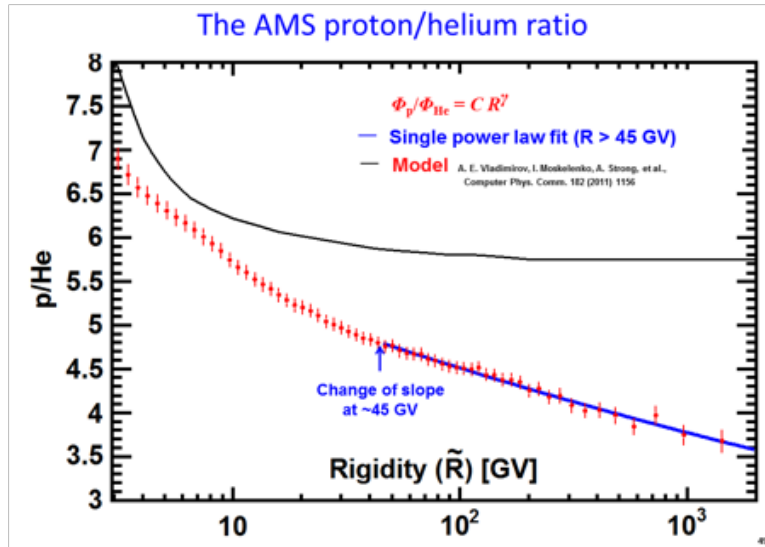


Figure 45: The AMS measurement of the proton/helium flux ratio.

The AMS measurement of the proton/helium flux ratio is shown in Figure 46 with the fit with of a single power law above 45 GV. Also shown are other recent measurements.

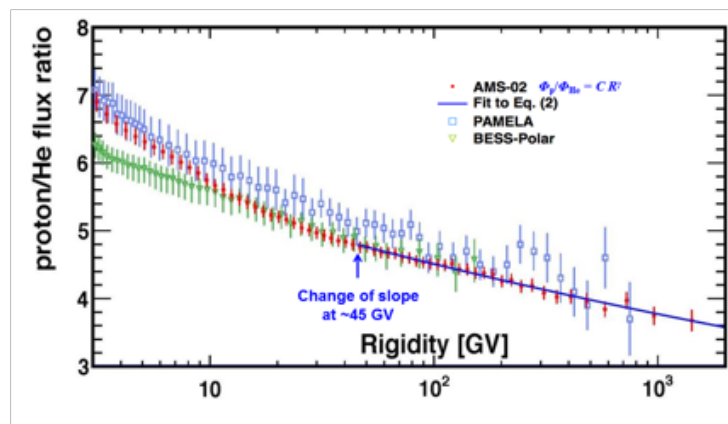


Figure 46: The AMS measurement of the proton/helium flux ratio fit with a single power law above 45 GV together with recent measurements.

Figure 47 shows the rigidity dependence of the proton/helium ratio spectral index,  $C \cdot R^{\gamma(p/He)}$ . As seen, above 45 GV the spectral index of the ratio is constant with  $\gamma_{p/He} = -0.077 + 0.002$  (fit)  $+ 0.007$  (sys).

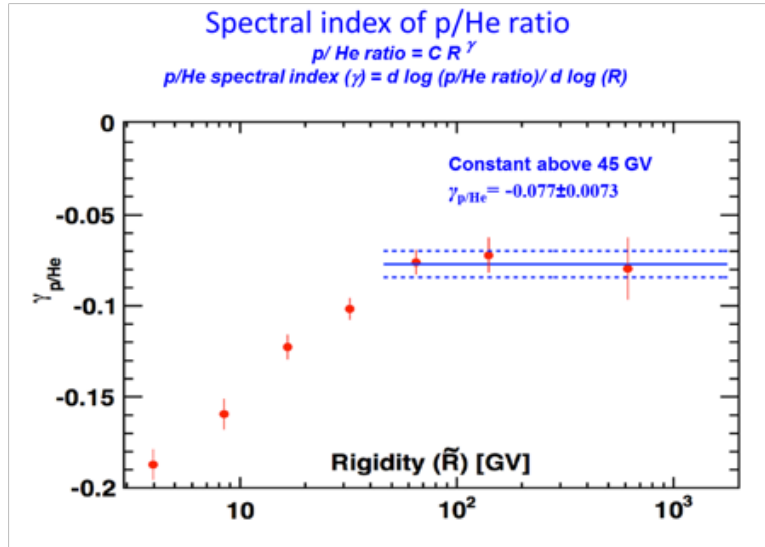


Figure 47: The spectral index of the proton/helium flux ratio fit with a constant above 45 GV.

The lithium flux measurement provides important information on the propagation of cosmic rays in the interstellar medium. Historically, lithium was assumed to be of purely secondary origin from the collision of primary cosmic rays with interstellar matter. Prior to AMS, data on the lithium flux was limited as shown in Figure 48. The current status of the AMS lithium flux measurement based on 1.5 million events is shown in Figure 49 together with the results of previous experiments [5].

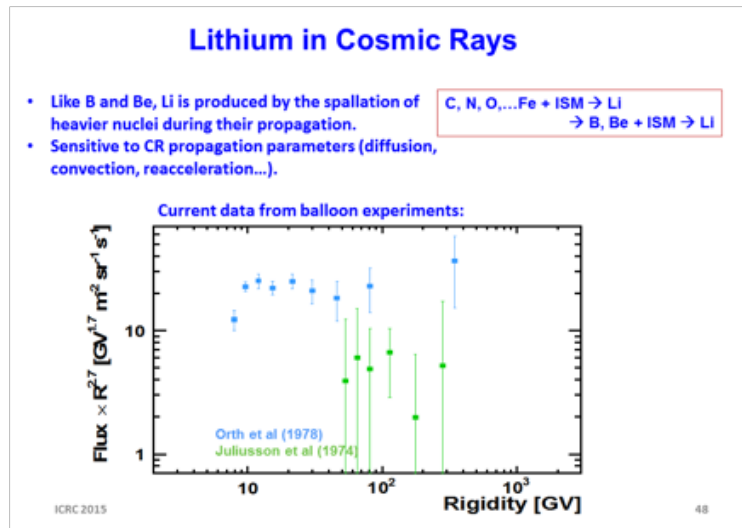


Figure 48: The importance of studying the lithium flux together with measurements before AMS of the flux of lithium before AMS multiplied by  $R^{2.7}$ .

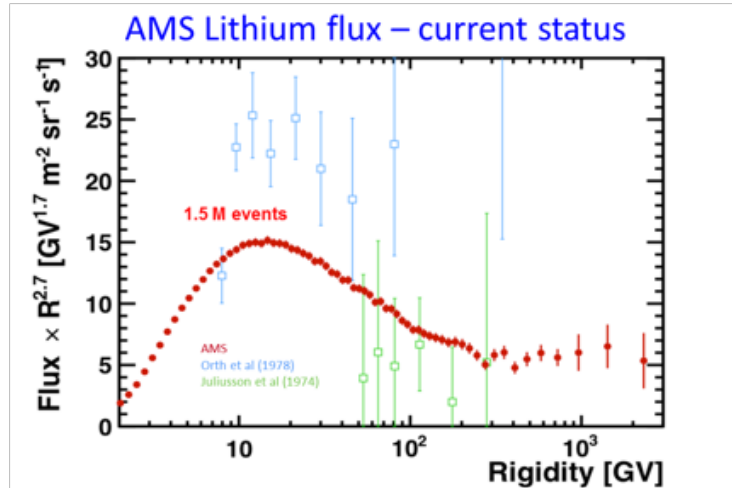


Figure 49: The current status of the AMS measurement of the lithium flux together with earlier measurements multiplied by R<sup>2.7</sup>.

As can be seen from Figure 50, the lithium flux cannot be described by a single power law,  $\Phi = CR^\gamma$ , as was always assumed. These results contradict the assumption that cosmic lithium is purely secondary in origin. Purely secondary production of lithium would not produce a deviation from a single power law. It is important to note that the accurate measurement of the lithium flux exhibits a change in slope at approximately the same rigidity as that observed for protons and helium, see Figure 34 and 42.

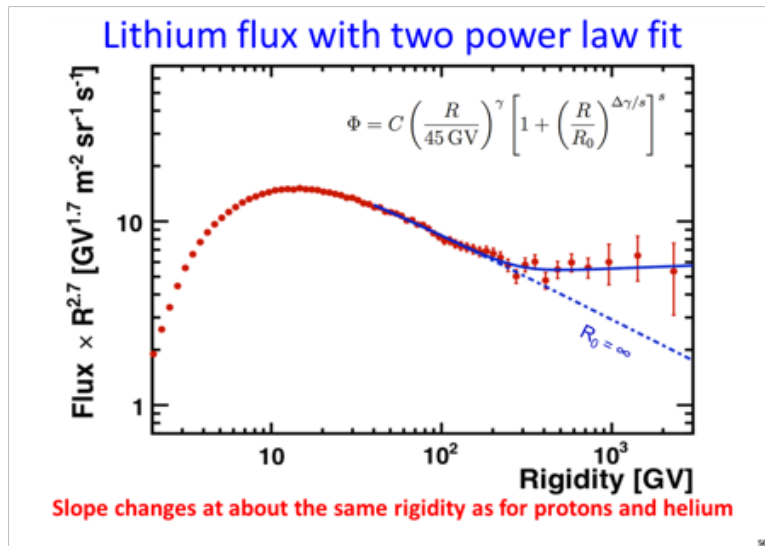


Figure 50: The AMS lithium flux multiplied by R<sup>2.7</sup> and fit with a double power law.

The boron-to-carbon ratio (B/C) in cosmic rays is a powerful tool to determine cosmic ray propagation as boron is assumed to be produced purely from collision of primary cosmic rays, such as carbon and oxygen, with the interstellar medium as illustrated in Figure 51. However, carbon nuclei can interact within AMS and appear as boron. The inset of Figure 51 shows the reconstruction of an event in which this happened. The first two measurements have  $Z=6$  then a large deposit consistent with an interaction and the subsequent measurements have  $Z=5$ . With AMS, these interactions can be carefully controlled as shown in Figure 52, the charge measured at the first layer of AMS vs the charge measured with the rest of the detector. This enables us to control the sample purity while maintaining high efficiency.

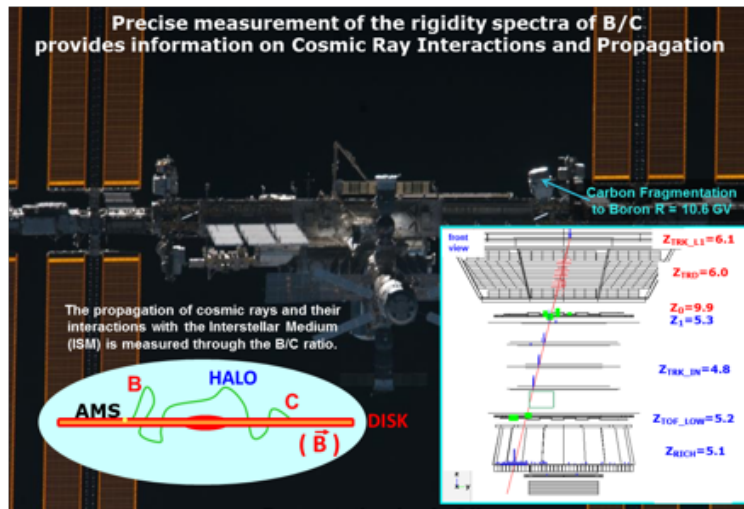


Figure 51: The importance of measuring the boron/carbon (B/C) ratio and (inset) the reconstruction of a carbon nuclei fragmenting into a boron nuclei within AMS.

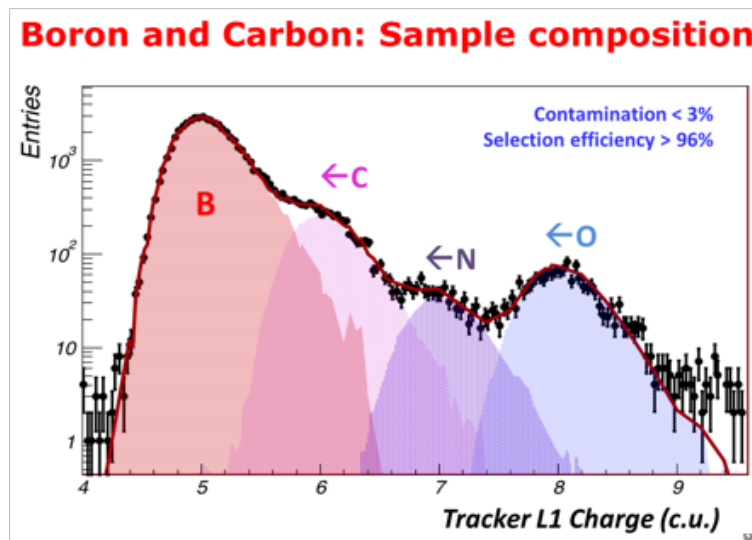


Figure 52: Selection and separation of boron and carbon with AMS.

The AMS results based on 7 million carbon and 2 million boron nuclei of the boron-to-carbon ratio vs energy are shown in Figure 53 together with earlier measurements [6].

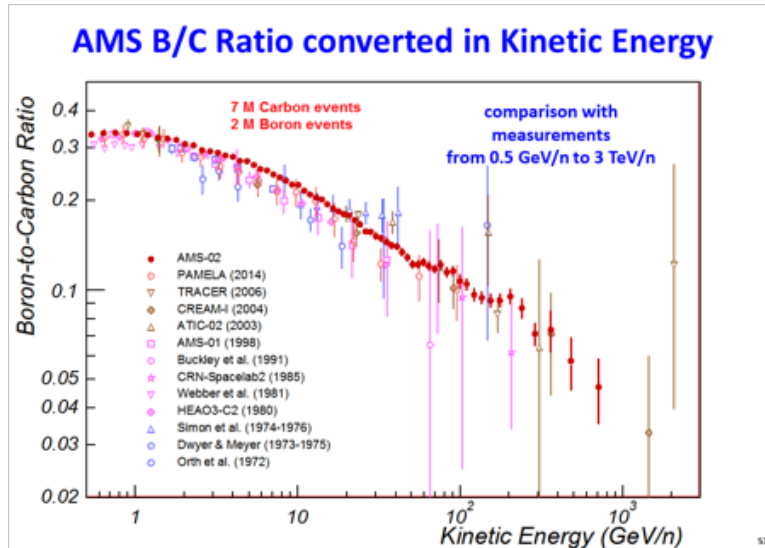


Figure 53: The AMS B/C ratio together with earlier measurements.

The exact behavior of the carbon flux with rigidity and how it relates to the behavior of the helium flux is important for understanding charge dependencies of the production, acceleration and propagation mechanisms of charged cosmic rays. The current status of the measurement of the carbon flux is shown in Figure 54 [7]. The current statistical precision of the data at highest energies is not sufficient to distinguish a single power law behavior of the carbon flux from a double power law behavior, as we observe for protons, helium and lithium.



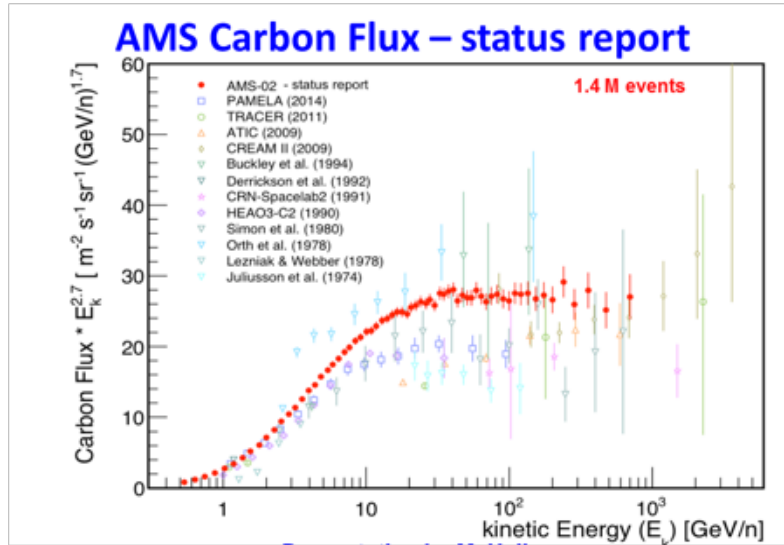


Figure 54: Status of the AMS measurement of the carbon flux.

#### 4. Conclusion

The latest AMS results have had an impact on the current understanding of cosmic rays. Figure 55 summarizes the physics of AMS and Figure 56 the importance of the Space Station in the study of fundamental physics.

The latest AMS measurements of the positron fraction, the antiproton/proton ratio, the behavior of the fluxes of electrons, positrons, protons, helium, and other nuclei is providing new, precise, and unexpected information.

The accuracy and characteristics of the data, simultaneously from many different types of cosmic rays, will soon determine the true nature of the new phenomena we observe.

**AMS physics for the lifetime of the Space Station**

Accurate measurement (~1%) of Cosmic Rays to higher energies including:

- Continue the study of Dark Matter
- Search for the Existence of Antimatter
- Search for New Phenomena, ...

55

Figure 55: Physics from AMS.

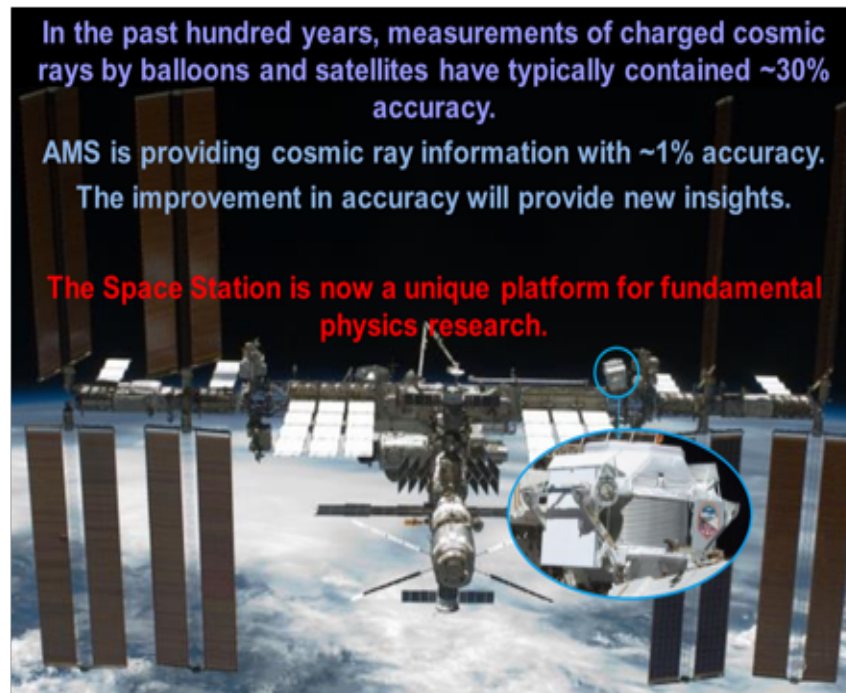


Figure 56: Concluding remarks.

## 5. Acknowledgements

I wish to acknowledge the organizers of this ICRC, particularly Prof. Dr. Ad. M. van den Berg and Prof. Dr. J. Horandel, for their excellent program and hospitality as well as my AMS colleagues M. Capell, V. Choutko, L. Derome, M. Duranti, A. Kounine, S. Haino, M. Heil, A. Oliva for providing detailed AMS results which I have summarized in this presentation.

**References**

- [1] A. Kounine, *Latest Alpha Magnetic Spectrometer results : positron fraction and  $p\bar{b}ar/p$  ratio*, in the proceedings of this conference; and references therein.
- [2] M. Duranti, *Precision Measurement of the  $(e^++e^-)$  Flux in Primary Cosmic Rays from 0.5 GeV to 1 TeV with the Alpha Magnetic Spectrometer on the International Space Station*, in the proceedings of this conference; and references therein.
- [3] V. Choutko, *Precision Measurement of the Proton Flux in Primary Cosmic Rays from 1 GV to 1.8 TV with the Alpha Magnetic Spectrometer on the International Space Station*, in the proceedings of this conference; and references therein.
- [4] S. Haino, *Precision Measurement of the Helium Flux in Primary Cosmic Rays from 2 GV to 3 TV with the Alpha Magnetic Spectrometer on the International Space Station*, in the proceedings of this conference; and references therein.
- [5] L. Derome, *Precision Measurement of Lithium Flux in Cosmic Rays with the Alpha Magnetic Spectrometer on the International Space Station*, in the proceedings of this conference; and references therein.
- [6] A. Oliva, *Precision Measurement of Boron to Carbon Flux Ratio in Cosmic Rays with energies from 0.5 GeV/n to 1 TeV/n with the Alpha Magnetic Spectrometer on the International Space Station*, in the proceedings of this conference; and references therein.
- [7] M. Heil, *Precision Measurement of the Carbon to Helium Flux Ratio in Cosmic Rays from 2 GV to 2 TV with the Alpha Magnetic Spectrometer on the International Space Station*, in the proceedings of this conference; and references therein.